VISCOUS AIR DAMPING IN LATERALLY DRIVEN MICRORESONATORS

Xia Zhang* and William C. Tang

Ford Microelectronics, Inc.
Colorado Springs, CO 80921

*also at Berkeley Sensor & Actuator Center
An NSF/University/Industry Cooperative Research Center
The University of California at Berkeley

ABSTRACT

A systematic experimental study of viscous air damping in laterally moving planar microstructures is reported. Previous studies indicated that Couette and Stokes flow models underestimated microstructural damping. To investigate this discrepancy, a series of lateral resonant microstructures with different damp plates and combs was fabricated with polysilicon surface micromachining. The resonant frequencies and quality factors of the structures were measured electrically. By examining these data, the damping due to different geometries were isolated and compared to theory. The results indicated that if edge and finite-size effects are included in the model, reasonably accurate prediction on the quality factors can be obtained even for small geometries and comb drives. An empirical formula was developed that predicts quality factor for a range of plate size and comb designs. The damping effects as a function of structural thickness and structure-to-substrate separation are also reported.

INTRODUCTION

Surface-micromachined, laterally driven microstructures have served as important research vehicles for many microactuators and microsensors [1]. In these devices, the damping level determines their amplitude response and stability, and therefore is a crucial parameter to their functionality. In contrast to vertically driven devices, in which squeeze film damping is the major source of energy dissipation [2], viscous drag of the ambient fluid is the dominant dissipative source in laterally driven structures. Damping in laterally moving microstructures was previously investigated with Couette [3,4] and Stokes flows [5] as the models. The estimated quality factor Q based on both models were consistently higher than the measured values.

In this paper, we report a systematic investigation on damping in laterally oscillating microstructures by including edge and finite-size effects. A series of electrostatically driven test devices was designed to isolate the effects of various geometrical attributes. An empirical formula is presented that predicts quality factor Q for a range of lateral microstructures.

THEORETICAL BACKGROUND

The microdynamical system under study can be modeled as a forced oscillating spring system with a viscous damper. A planar mass M, driven by a periodic force $F(t)$, is subjected to a restoring force from a suspension with spring constant k, and a damping force with damping coefficient c.

For the one-sided single-folded beam structure, the spring constant is given by [6]

$$k = \frac{12EI}{l^3} = Eh\left(\frac{w}{l}\right)^3 \qquad (1)$$

where $I = (hw^3/12)$ is the moment of inertia of the beams, h, w, and l are the thickness, width, and length of the beams, respectively, and E is the Young's modulus. The undamped natural frequency (f_r) of this system is given by

$$f_r = \frac{1}{2\pi}\sqrt{\frac{k}{M}} = \frac{1}{2\pi}\sqrt{\frac{Ew^3}{\rho l^3 A_M}} \qquad (2)$$

The effective mass of the system, M, is related to the effective area, A_M:

$$M = \rho h A_M = \rho h\left(A_p + \frac{1}{4}A_t + \frac{12}{35}A_b\right) \qquad (3)$$

where A_p, A_t, and A_b are the top areas of the plate, the outer truss, and the supporting beams, respectively.

Some of the energy dissipative processes in a lateral moving microstructure are shown schematically in Fig. 1. In general, when the characteristic dimension of the structure d (related to the minimum feature size and thickness of the structure, and the thickness of the fluid layer) is much larger than the mean free path of the ambient gas λ ($d > 100\lambda$), the flow is within the continuum regime. When ($d < \lambda$), the flow is in the molecular regime. The intermediate region ($\lambda < d < 100\lambda$) is called Knudsen flow.

Since the characteristic dimension of our test structures is $d = 2$ µm, and with air at one atmosphere and room temperature $\lambda = 0.06$ µm, we have ($d \approx 33\lambda$). The flow is in the marginal region between the continuum and Knudsen

0-7803-1833-1/94 $3.00 © 1994 IEEE

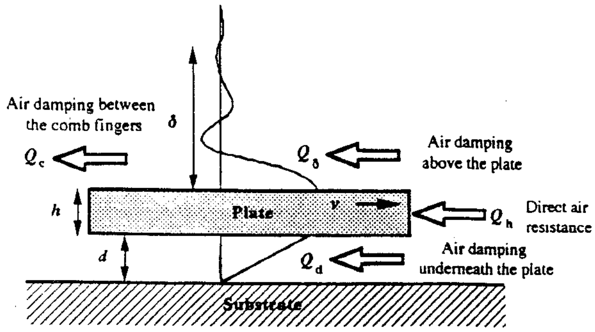

Figure 1 Dissipative processes in a lateral resonator.

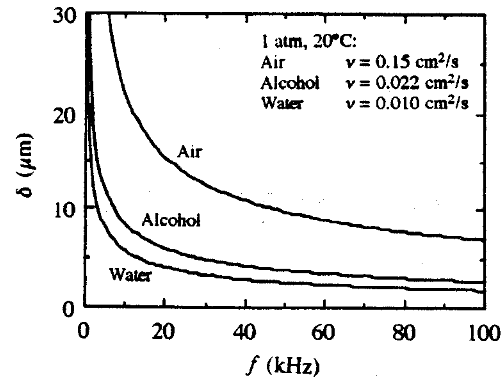

Figure 2 Penetration depth δ as a function of frequency f.

regimes. Since Knudsen flow is difficult to characterize analytically, we will assume continuum flow in our analysis, which predicts laminar flow in the fluid layers surrounding the moving structures. This assumption will be examined in light of experimental results.

With this assumption, the fluid between two parallel plates in relative motion undergoes Couette flow with a linear velocity profile. The quality factor due to Couette flow alone, Q_d, with fluid thickness d, is given by [7]

$$\frac{1}{Q_d} = \frac{\mu A_q}{d\sqrt{Mk}} = \frac{2\pi f_r \mu A_q}{dk} \tag{4}$$

where μ is the absolute viscosity of the ambient fluid, and A_q is the damping-related effective area of the system, given by $A_q = A_p + 0.5\,(A_t + A_b)$.

The motion of the fluid on top of the plate can be modeled as Stokes flow [5], in which the amplitude of fluid oscillation decays exponentially with the distance from the plate surface, while phase lag increases linearly. The *penetration depth*, δ, which is defined as the distance at which the motion amplitude of the fluid decreases by a factor of e, is given by [8]:

$$\delta(\omega) = \sqrt{\frac{2\upsilon}{\omega}} \tag{5}$$

where $(\upsilon = \mu/\rho)$ is the kinetic viscosity of the fluid. Equation (5) implies that a slow oscillating plate in a viscous medium is expected to drag substantially more amount of fluid compared to a fast moving one in a fluid of low viscosity. Penetration depth is plotted as a function of oscillating frequency for some common fluids in Fig. 2.

A practical use of δ is that the fluid beyond the penetration depth may be assumed stationary. Thus Stokes flow on the top surface can be approximated with the Couette formula by replacing d with δ, provided that the oscillation frequency is moderately low. With this approximation, the quality factor due to drag on the top surface alone (Q_δ) is

$$\frac{1}{Q_\delta} \approx \frac{2\pi f_r \mu A_\delta}{\delta k} \tag{6}$$

This contribution is roughly 10% of that from Couette damping (for $d = 2\ \mu\text{m}$, $f_r = 10$ kHz, air).

To account for the quality factor (Q_c) related to damping between the comb fingers, Eq. (4) can be used again [5]

$$\frac{1}{Q_c} \approx \frac{2\pi f_r \mu A_c}{d_c k} \tag{7}$$

where A_c is the area of the comb finger overlap, and d_c is the comb gap.

The overall quality factor Q can be obtained by combining Eqs. (4), (6), and (7):

$$\frac{1}{Q} = \sum \frac{1}{Q_i} = \frac{\mu}{\sqrt{E\rho A_M \left(\frac{w}{l}\right)^3}} \left(\frac{A_q}{dh}\left(1 + \frac{d}{\delta}\right) + \frac{A_c}{d_c h}\right) \tag{8}$$

Since Q is a function of both A_M and A_q, damping effects due to different geometry (A_q) cannot be obtained from direct comparison of Q alone. Instead, we use the quantity ($1/Qf_r$) for comparison:

$$\frac{1}{Qf_r} = \frac{2\pi\mu}{E\,(w/l)^3} \left(\frac{A_q}{dh}\left(1 + \frac{d}{\delta}\right) + \frac{A_c}{d_c h}\right) \tag{9}$$

Note that A_M is factored out from this expression. Since E and (w/l) are designed to be the same, the damping contributions from different geometries can be separated.

Finally, it should be noted that due to finite process nonuniformity across the wafer, the structures from different dies of the same wafer are not identical. Also, variations of both f_r and Q are mainly results of variation in w across the wafer. However, the quantity (f_r/Q) is almost constant for the same design from die to die:

$$\frac{f_r}{Q} = \frac{\mu}{2\pi\rho A_M} \left(\frac{A_q}{dh}\left(1 + \frac{d}{\delta}\right) + \frac{A_c}{d_c h}\right) \tag{10}$$

which is independent of E and w. This suggests a way to average the quantity ($1/Qf_r$) obtained for the same design on different dies for better comparison.

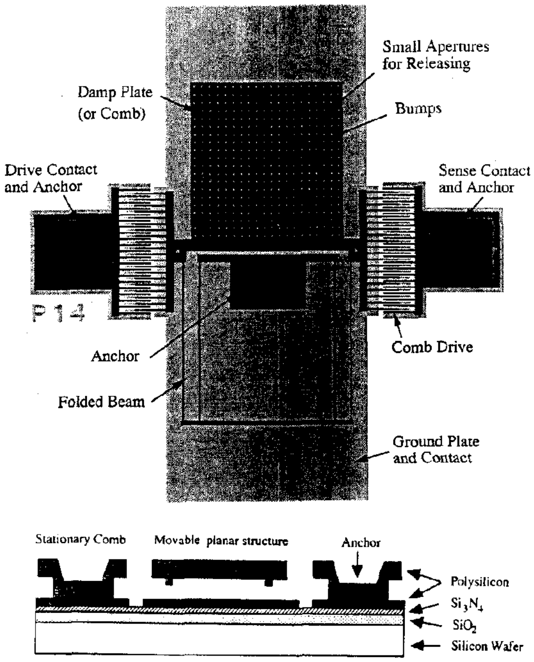

Figure 3 Layout and cross section of a lateral resonator.

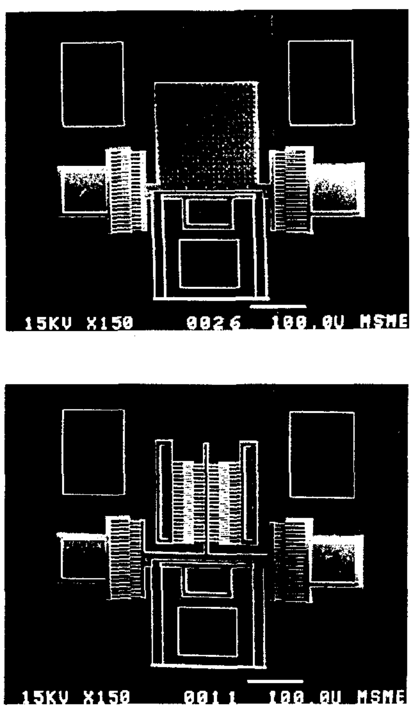

Figure 4 SEM micrographs of test structures (P4 and C).

EXPERIMENTAL RESULTS

Design of test structures

The layout and cross-sectional view of one of the test devices is shown in Fig. 3. The ground plate is used to reduce the vertical levitation effect [9]. All structures have identical, one-side-only single-folded beam suspension and 20-finger drive and sense combs. The first group (P series) of test structures have damp plates of various sizes. The second group of test structures have damp combs with various numbers of fingers, with (C series) or without (D series) the outside fixed comb fingers. SEM micrographs of some of the completed structures are shown in Fig. 4.

Characterization technique

The test devices are driven into lateral motion with an ac signal (20 V p–p) on top of a 20 V dc bias applied to one of the fixed combs (drive port) [3]. The displacement current caused by the motion is detected by sensing at the other comb (sense port) with the electromechanical amplitude modulation (EAM) method [10]. A recorded spectrum of resonant amplitude as a function of frequency is shown in Fig. 5. From this plot, both f_r and Q can be obtained. The oscillating amplitudes at resonance are within the range of 8 to 12 μm. Tests indicate that the influence of resonant amplitude on f_r and Q is not observable. Measurements for the same structure are repeated in ten different dies and averaged.

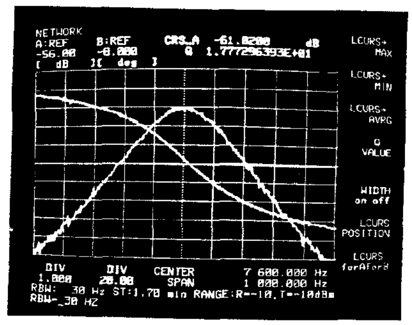

Figure 5 The measured amplitude and phase response curves.

For the P0 structures, the dimensions and its characteristics calculated with Eqs. (1–3) and (8) are listed in Table 1. The values E = 140 GPa and ρ = 2.33 g·cm^{-3} are used in the calculations.

The measured f_r is 11.7 ± 0.2 kHz, and Q is 16.6 ± 0.4. Results measured from other units are all in close agreement with the calculated values, with Q being consistently lower than that predicted with the Stokes theory.

Damping due to plate geometries

First, we study the damping contribution from plate geometries. The structures P0–P6 have plate areas varying from 0 to 6 × 10^4 μm^2 in increment of 1 × 10^4 μm^2. The

Table 1: Dimension and estimated characteristics of the P0 series. All quantities, except those followed by *, are the same for all structures.

beam width (w)	2.0 µm
beam length (l)	200 µm
structure thickness (h)	2.1 µm
air film thickness (d)	2.1 µm
finger width (w_c)	2.0 µm
finger gap (d_c)	2.0 µm
plate area (A_p) *	1.04×10^4 µm^2
truss area (A_t)	0.11×10^4 µm^2
beam area (A_b)	0.16×10^4 µm^2
finger area (A_c) *	0.32×10^4 µm^2
effective mass area (A_M) *	1.12×10^4 µm^2
effective damp area (A_q) *	1.18×10^4 µm^2
spring constant (k)	0.28 µN·µm^{-1}
effective mass (M) *	0.052 µg
resonant frequency (f_r) *	11.65 kHz
quality factor (Q) *	26.3

measured Q and ($1/Qf_r$) are plotted in Fig. 6. It can be seen that Q does not vary linearly with plate area, while ($1/Qf_r$) does. Table 2 compares the average change in ($1/Qf_r$) for an increase of 1×10^4 µm^2 in area. From Eqs. (4) and (6):

$$\Delta\left(\frac{1}{Qf_r}\right) = \frac{2\pi\mu}{E\left(\frac{w}{l}\right)^3} \frac{\Delta A_q}{dh}\left(1 + \frac{d}{\delta}\right) \tag{11}$$

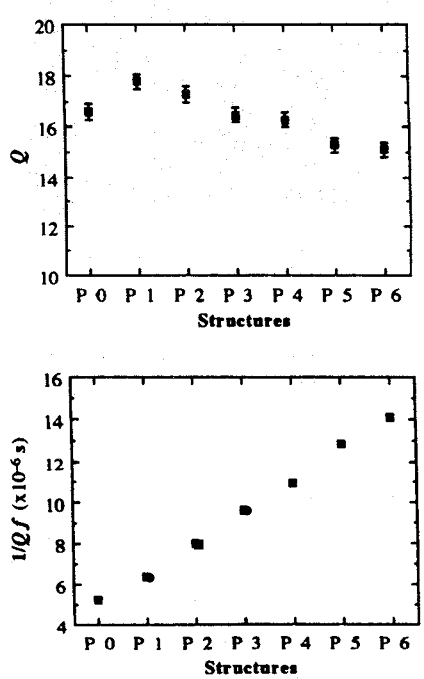

Figure 6 Measured Q and ($1/Qf_r$) for structures Px.

Table 2: Measured and estimated $\Delta(1/Qf_r)$ for Px

Structure	Measured $\Delta(1/Qf_r)$ [10^{-6} Hz^{-1}]	Estimated $\Delta(1/Qf_r)$ [10^{-6} Hz^{-1}]
P(x+1) − Px	1.5 ± 0.3	1.8

Damping due to comb fingers

Second, we study the damping contribution from comb fingers. Test structure C has 20 comb fingers on each side plus two sets of stationary fingers. The structure D is identical to C, except that the fixed fingers are removed. The structure C0 has the central truss only. The results are listed in Table 3.

Table 3: Measured results for C, D, and C0

Structure	f_r [kHz]	Q	$1/Qf_r$ [10^{-6} Hz^{-1}]
C0	10.7	15.0	6.2
D	9.6	13.5	7.7
C	9.6	12.8	8.1

A full set of comb structures contribute to damping in several ways: increasing the plate damping (A_q), generating inter-comb damping by increasing A_c, as well as providing possible squeeze film damping between the moving and fixed fingers (not included in the theory). By comparing the results of D and C0, the damping effects produced by comb structures to the area A_q as plate damper can be obtained; and by contrasting ($1/Qf_r$) for C and D, inter-comb damping due to the presence of the fixed fingers can be separated. The sum of them is the total damping contribution of a full comb structure, which is also measured by the difference of ($1/Qf_r$) between C and C0. Results are listed in Table 4 for comparison. Also included is the result of subtracting $1/Qf_r$ for C0 and P0, which gives the damping contribution of a small planar structure—the central truss of 10 µm ×220 µm.

Table 4: Measured and estimated $\Delta(1/Qf_r)$ for C, D, C0, P0

Structure	Measured $\Delta(1/Qf_r)$ [10^{-6} Hz^{-1}]	Estimated $\Delta(1/Qf_r)$ [10^{-6} Hz^{-1}]
C − C0	1.9 ± 0.3	1.2
D − C0	1.5 ± 0.3	0.6
C − D	0.4 ± 0.3	0.6
C0 − P0	0.8 ± 0.3	0.4

Direct air resistance

Third, we investigate the effects that are related to the detailed geometry of the structure. The 50 µm x 200 µm damp plates for structures P1 and X1 are oriented 90° relative to each other. In P1, the long side of the plate is along the direction of motion, while in X1 the long side is facing the motion direction. The results are listed in Table 5.

Table 5: Measured results for P1 and X1

Structure	f_r [kHz]	Q	$1/Qf_r$ [10^{-6} Hz^{-1}]
P1	8.8	17.8	6.4
X1	8.8	17.0	6.7

Comparing P1 and X1, we have $\Delta(1/Qf_r) = (0.3 \pm 0.1) \times 10^{-6}$ Hz^{-1}. Consistent with theoretical reasoning, X1, with a larger area perpendicular to the direction of motion, has a slightly larger damping. This damping is most probably a result of direct air resistance. It is reasonable to assume that this term (Q_h) is velocity-squared damping, and it is proportional to the density of the fluid ρ_f and the cross section area facing the direction of motion.

Dependence of damping on *d* and *h*

Finally, the effects of air film thickness d and structure thickness h on the damping are studied. Different d and h are fabricated with values at 2.1, 3.1, and 4.1 μm. Q and f_r are measured for the same design P2 from a total of nine d and h combinations. Although Eq. (2) predicts that the resonant frequency is independent of both d and h in theory, the measured values for f_r increase slightly with increasing h and d, probably a result of increasing effective w with increasing h (a process limitation). To eliminate this effect, the measured f_r and Q for all combinations are scaled to the frequency $f_r = 7.2$ kHz (at $d = 2.1$ μm and $h = 2.1$ μm). The values of Q for P2 are plotted as a function of d and h in Fig. 7. When d (or h) increases from 2.1 to 4.1 μm, Q increases by a factor of 1.3 (or 1.6).

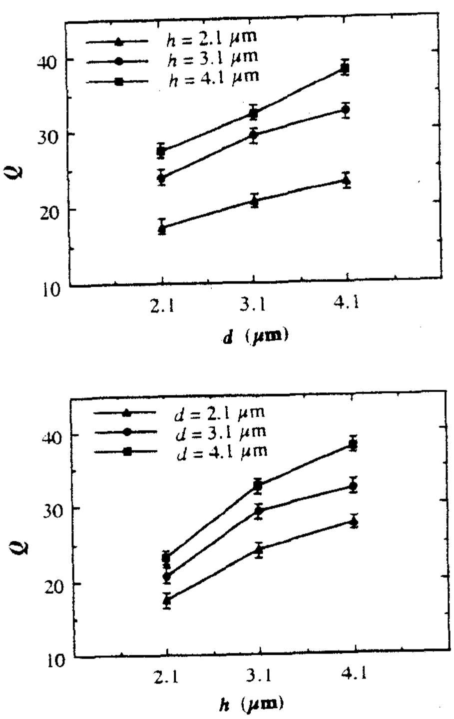

Figure 7 Measured Q as functions of separation d and film thickness h.

DISCUSSIONS

Edge and finite-size effects

Experimental results indicate that the Stokes theory agrees reasonably well with the experimental results for large damp plates (P series), but failed for small dimension (C0) and comb structures (C and D). The measured damping by the central truss in C0 is twice the estimated value. Damp combs introduce a significant amount of damping, which decreases only slightly when the fixed fingers are removed. The measured contribution from comb fingers in D is 2.5 times the theoretical value. Inter-comb damping (obtained by comparing C and D) is described well by Eq. (7), and the squeeze film damping or pumping effect, if any, must be negligible.

For a moving plate of finite area, the penetration depth is better described with the boundary layer theory [11], as shown in Fig. 8. The penetration depth is smaller at the leading edge, and additional fluid volume is dragged behind the trailing edge [12]. This suggests an edge effect which becomes significant for small structures.

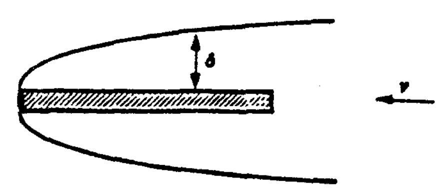

Figure 8 Boundary layer thickness over a flat plate of finite size.

A moving plate of finite area also drags additional fluid volume along its sides, again resulting in additional damping for small dimension structures, a finite-size effect. Both the finite-size and edge effects are most prominent in comb structures, which are regular arrays of small dimension fingers. An alternative in examining comb structures is to use the area outlined by the outer boundary of the comb (subtracting areas for fixed fingers) for damping calculation, which would include both the area of the fingers and the finger gaps. This results in a calculated value much closer to the measured value. Theoretically, it is quite reasonable to assume that the fluid volumes above both the comb fingers and the finger gaps are dragged into motion due to their proximity.

Empirical formula for *Q* estimation

Taking edge and finite-size effects into consideration, the damping generated by plate geometries can be generalized as

$$\frac{1}{Q} = \frac{\mu}{\sqrt{E\rho A_M (w/l)^3}} \frac{\alpha A_q}{dh} \left(1 + \frac{d}{\delta}\right) \tag{12}$$

Table 5: Measured results for P1 and X1

Structure	f_r [kHz]	Q	$1/Qf_r$ [10^{-6} Hz^{-1}]
P1	8.8	17.8	6.4
X1	8.8	17.0	6.7

Comparing P1 and X1, we have $\Delta(1/Qf_r) = (0.3 \pm 0.1) \times 10^{-6}$ Hz^{-1}. Consistent with theoretical reasoning, X1, with a larger area perpendicular to the direction of motion, has a slightly larger damping. This damping is most probably a result of direct air resistance. It is reasonable to assume that this term (Q_h) is velocity-squared damping, and it is proportional to the density of the fluid ρ_f and the cross section area facing the direction of motion.

Dependence of damping on *d* and *h*

Finally, the effects of air film thickness d and structure thickness h on the damping are studied. Different d and h are fabricated with values at 2.1, 3.1, and 4.1 µm. Q and f_r are measured for the same design P2 from a total of nine d and h combinations. Although Eq. (2) predicts that the resonant frequency is independent of both d and h in theory, the measured values for f_r increase slightly with increasing h and d, probably a result of increasing effective w with increasing h (a process limitation). To eliminate this effect, the measured f_r and Q for all combinations are scaled to the frequency f_r = 7.2 kHz (at d = 2.1 µm and h = 2.1 µm). The values of Q for P2 are plotted as a function of d and h in Fig. 7. When d (or h) increases from 2.1 to 4.1 µm, Q increases by a factor of 1.3 (or 1.6).

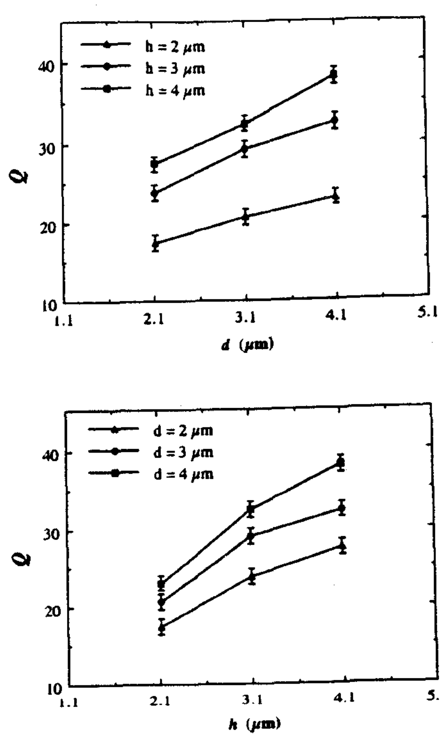

Figure 7 Measured Q as functions of separation d and film thickness h.

DISCUSSIONS

Edge and finite-size effects

Experimental results indicate that the Stokes theory agrees reasonably well with the experimental results for large damp plates (P series), but failed for small dimension (C0) and comb structures (C and D). The measured damping by the central truss in C0 is twice the estimated value. Damp combs introduce a significant amount of damping, which decreases only slightly when the fixed fingers are removed. The measured contribution from comb fingers in D is 2.5 times the theoretical value. Inter-comb damping (obtained by comparing C and D) is described well by Eq. (7), and the squeeze film damping or pumping effect, if any, must be negligible.

For a moving plate of finite area, the penetration depth is better described with the boundary layer theory [11], as shown in Fig. 8. The penetration depth is smaller at the leading edge, and additional fluid volume is dragged behind the trailing edge [12]. This suggests an edge effect which becomes significant for small structures.

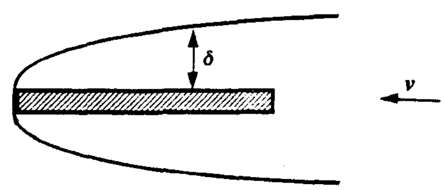

Figure 8 Boundary layer thickness over a flat plate of finite size.

Comparing P1 and X1, we have $\Delta(1/Qf_r) = (0.3 \pm 0.1) \times 10^{-6}$ Hz^{-1}. Consistent with theoretical reasoning, X1, with a larger area perpendicular to the direction of motion, has a slightly larger damping. This damping is most probably a result of direct air resistance. It is reasonable to assume that this term (Q_h) is velocity-squared damping, and it is proportional to the density of the fluid ρ_f and the cross section area facing the direction of motion.

Dependence of damping on *d* and *h*

Finally, the effects of air film thickness d and structure thickness h on the damping are studied. Different d and h are fabricated with values at 2.1, 3.1, and 4.1 µm. Q and f_r are measured for the same design P2 from a total of nine d and h combinations. Although Eq. (2) predicts that the resonant frequency is independent of both d and h in theory, the measured values for f_r increase slightly with increasing h and d, probably a result of increasing effective w with increasing h (a process limitation). To eliminate this effect, the measured f_r and Q for all combinations are scaled to the frequency f_r = 7.2 kHz (at d = 2.1 µm and h = 2.1 µm). The values of Q for P2 are plotted as a function of d and h in Fig. 7. When d (or h) increases from 2.1 to 4.1 µm, Q increases by a factor of 1.3 (or 1.6).

where α is a scaling factor. When the dimension of the plate is large compared to the air film thickness, the assumption of infinite plate is acceptable, i.e. (α = 1). With small dimension plates, α depends on the design of the plates, and is greater than one. Empirically, ($\alpha \approx 3$) is appropriate for comb structures, and ($\alpha \approx 2$) is suitable for other small dimension structures (with dimension 2 to 10 μm).

Combining the results of Eq. (8) and (12), we have the following expression for the overall Q

$$\frac{1}{Q} = \frac{\mu}{\sqrt{E\rho A_M (w/l)^3}} \left(\frac{\alpha A_q}{dh} (1 + \frac{d}{\delta}) + \frac{A_c}{d_c h} \right) + \frac{1}{Q_h} \quad (13)$$

where Q_h is the term to account for direct air resistance.

Using Eq. (13), Q for structure P0 can be recalculated (see Table 6). If Q_h is ignored, we have Q = 17.2. A contribution of ($1/Q_h = 2 \times 10^{-3}$) will give Q = 16.6, which is the measured value. Equation (13) also gives satisfactory estimations of Q for all other structures. It can also be used to explain the behavior of Q as a function of d and h, which is reflected by the second and third terms.

Table 6: Estimation of Q for P0

Term	Damping elements	Area [10^3 μm^2]	α	1/Q [10^{-2}]
1	large areas (central and finger bars)	7.2	1	1.87
1	small areas (beam and truss)	1.4	2	0.72
1	small areas (comb fingers)	3.2	3	2.48
2	inter-comb fingers	3.2	–	0.75
3	direct air resistance	est.	–	0.20
Total				6.02

CONCLUSIONS

We have investigated experimentally and theoretically various mechanisms of viscous air damping in laterally oscillating planar microstructures. The results indicate that a better agreement between experiment and theory can be obtained by including edge and finite-size effects to the Couette and Stokes theories. This is especially useful for modeling Q of small structures and comb drives. Also when the characteristic dimension of the structure d is not too small, using continuum flow theory is a good approximation, even for the cases with $d \approx 33\lambda$. Future research will be in the area of 3D finite-element modeling of small-size and edge effects of viscous damping.

ACKNOWLEDGMENTS

This work was supported by Ford Motor Company. The test structures were fabricated in Berkeley Microfabrication Laboratory. We would like to thank members of Berkeley Sensor & Actuator Center for their hospitality during the visit of one of us (XZ) as an industry research fellow.

REFERENCES

[1] See, for example, *Microsensors*, edited by R. S. Muller, *et al*, New York: IEEE Press, 1991.

[2] M. Andrews, I. Harris, and G. Turner, "A comparison of squeeze-film theory with measurements on a microstructure," *Sensors and Actuators*, vol. A36, pp. 79–87, 1993.

[3] W. C. Tang, T. -C. H. Nguyen, and R. T. Howe, "Laterally driven polysilicon resonant micro-structures," *Sensors and Actuators*, vol. 20, pp. 25–32, 1989.

[4] W. C. Tang, T. -C. H. Nguyen, M. W. Judy, and R. T. Howe, "Electrostatic comb drive of lateral polysilicon resonators," *Sensors and Actuators*, vol. A21–23, pp. 328–331, 1990.

[5] Y.-H. Cho, B. M. Kwak, A. P. Pisano, and R. T. Howe, "Viscous energy dissipation in laterally oscillating planar microstructures: A theoretical and experimental study," *Proc. IEEE Workshop on Microelectromech. Sys.*, pp. 93–98, 1993.

[6] W. C.-K. Tang, "Electrostatic comb drive for resonant sensor and actuator applications", Ph.D. Thesis, Dept. EECS, Univ. of California, Berkeley, 1990.

[7] M. A. Schmitt, R. T. Howe, S. D. Senturia, and J. H. Haritonidis, "Design and calibration of a microfabricated floating-element shear-stress sensor," *IEEE Trans. Electron Devices*, vol. ED-35, pp. 750–757, 1988.

[8] W. E. Langlois, *Slow viscous flow,* New York: The Mcmillan Company, 1964.

[9] W. C. Tang, M. G. Lim, and R. T. Howe, "Electrostatic comb drive levitation and control method" *J. Microelectromech. Sys.*, vol. 1, pp. 170–178, 1992.

[10] T.-C. Nguyen, "Electromechanical characterization of microsensors for circuit application," Master Thesis, Dept. EECS, Univ. of California, Berkeley, 1991.

[11] H. Schlichting, *Boundary Layer Theory,* 7th ed. New York: McGraw-Hill, 1979.